

Ignition delay of a pulsed inductively coupled plasma (ICP) in tandem with an auxiliary ICP

Lei Liu, Shyam Sridhar, Vincent M Donnelly and Demetre J Economou

Plasma Processing Laboratory, Department of Chemical and Biomolecular Engineering, University of Houston, Houston, TX 77204, USA

E-mail: vmdonnelly@uh.edu and economou@uh.edu

Received 29 July 2015, revised 24 September 2015

Accepted for publication 29 September 2015

Published 3 November 2015



Abstract

Plasma ignition delays were observed in a ‘main’ inductively coupled plasma (ICP), in tandem with an ‘auxiliary’ ICP. The Faraday-shielded ICPs were separated by a grounded metal grid. Power (13.56 MHz) to the main ICP was pulsed with a frequency of 1 kHz, while the auxiliary ICP was operated in continuous wave (cw) mode. In chlorine plasmas, ignition delay was observed for duty cycles greater than 60% and, in contrast to expectation, the delay was longer with increasing duty cycle up to ~99.5%. The ignition delay could be varied by changing the auxiliary and/or main ICP power. Langmuir probe measurements provided the temporal evolution of electron temperature, and electron and positive ion densities. These measurements revealed that the plasma was ignited shortly after the decaying positive ion density (n_+), in the afterglow of the main ICP, reached the density ($n_{+,aux}$) prevailing when only the auxiliary ICP was powered. At that time, production of electrons began to dominate their loss in the main ICP, due to hot electron injection from the auxiliary ICP. As a result, n_e increased from a value below $n_{e,aux}$, improving inductive power coupling efficiency, further increasing plasma density leading to plasma ignition. Plasma ignition delay occurred when the afterglow of the pulsed plasma was not long enough for the ion density to reach $n_{+,aux}$ during the afterglow. Besides Cl_2 , plasma ignition delays were also observed in other electronegative gases (SF_6 , CF_4/O_2 and O_2) but not in an electropositive gas (Ar).

Keywords: inductively coupled plasma, pulsed plasma, plasma diagnostics

(Some figures may appear in colour only in the online journal)

1. Introduction

Pulsed plasmas are increasingly being developed for etching processes used to manufacture advanced semiconductor devices [1–4]. Compared to traditional continuous wave (cw) plasmas, pulsed plasmas offer added control of plasma parameters that affect etching characteristics such as selectivity, uniformity, anisotropy, and charging damage [5–14]. For example, Sugai *et al* [13] reported that by changing the duty cycle of a pulsed CF_4/H_2 plasma, the number density ratio of CF_x/F ($x = 2, 3$) could be controlled, which enabled control of selectivity of etching Si over SiO_2 , or vice versa. Samukawa *et al* [15, 16] demonstrated that better anisotropy and selectivity,

with less damage and more precise critical dimension control, can be obtained in Si etching using pulsed chlorine-containing plasmas. In addition, pulsed electronegative plasmas can reduce or eliminate undesirable etching anomalies (such as notching or bowing) caused by differential charging in features, by injecting negative charges into the bottom of the features to neutralize accumulated positive ion charge [15, 17].

More recently, pulsed plasmas have also been employed to obtain nearly monoenergetic ion energy distributions (IEDs) for improved control of ion-bombardment-stimulated processes, especially near the energy threshold [18]. Monoenergetic IEDs are critical for achieving very high selectivity of etching one material relative to another. In standard

radio frequency (RF) inductively coupled plasmas (ICPs), the substantial voltage across the coil capacitively couples to the plasma. This imposes an RF component on the dc plasma potential, broadening the ion energy distribution (IED) on the substrate during the power-on fraction of the cycle [1]. This IED broadening can be eliminated with a Faraday shield to block capacitive coupling. Especially with pulsed electronegative plasmas, however, it is very difficult to ignite the plasma in the next pulse cycle, since the electron density rapidly decays in the temporal afterglow (when power is off) by attachment and diffusion to the walls. Thus, ignition requires large electric fields produced by high-voltage capacitive coupling, which is suppressed by the Faraday shield.

In this work, we explored the use of an auxiliary plasma operating in tandem with a main plasma. Both sources were Faraday shielded. The auxiliary source was added to provide a flux of energetic electrons to the afterglow of the main source, allowing ignition without capacitive coupling. Although the auxiliary source enabled the prompt ignition of pulsed Ar plasmas under all conditions, with electronegative plasmas, a delay in ignition with respect to commencement of power was observed in the main source, under certain operating conditions.

Ignition delays in pulsed CF_4/Ar ICPs in the absence of a Faraday shield have been reported by Wang *et al* [19], and attributed to a capacitive-to-inductive (E–H) mode transition. Tuszewski [20] reported instabilities in low pressure electronegative discharges. Liebermann [21] and Chabert [22, 23] subsequently showed, using a global model, that these instabilities were a result of E–H transitions. E–H transition instabilities were attributed to differences in the production/loss rate of electrons and negative ions, causing the plasma to oscillate between inductive and capacitive discharge modes. Electron density builds up rapidly due to ionization and a quasi-equilibrium ‘inductive’ state (high electron density) of discharge is attained. Negative ion density continues to increase at a much slower rate, disturbing the equilibrium. Electrons are then lost rapidly due to attachment and the discharge reverts to a quasi-equilibrium low electron density ‘capacitive’ mode. Negative ions are lost at a much slower rate until the inductive mode is re-established [21–23]. In the present study, the ignition delay was not caused by an E–H mode transition since both plasma sources were equipped with a Faraday shield that precluded the E mode of the discharge. Systematic experiments were carried out to uncover the origin of the plasma ignition delay and its dependence on operating conditions.

2. Experimental

Figure 1 shows a schematic of the apparatus, consisting of two co-axial (tandem) plasmas. The main ICP (lower plasma) was an inductively coupled source powered by a 3-turn spiral coil in a 17.8 cm long, 8.6 cm inside diameter Al_2O_3 tube. The discharge tube was connected to a cubical stainless steel chamber through a water-cooled adaptor flange. The 5.08 cm diameter water-cooled stainless steel sample stage had a 2.64 cm diameter hole in the centre, allowing a Langmuir probe to

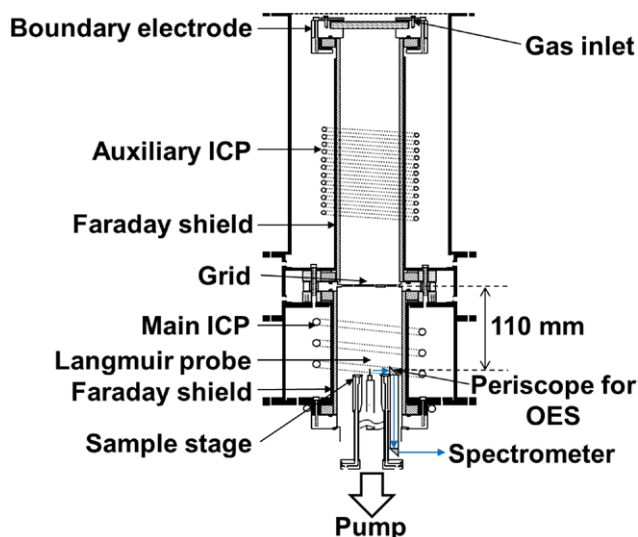


Figure 1. Schematic of the experimental apparatus. The main inductively coupled plasma (ICP) and the tandem auxiliary ICP were Faraday-shielded. The main ICP 13.56 MHz power was pulsed with a period of $1000 \mu\text{s}$ (1 kHz), while the auxiliary ICP 13.26 MHz power was applied continuously (cw mode). The axisymmetric sources were separated by a grounded metal grid. Optical emission was collected, through a periscope, from the main ICP, 110 mm below the grid. Langmuir probe measurements were performed on axis, also 110 mm below the grid.

pass through. An auxiliary ICP (upper plasma) was ignited by a 11.5-turn coil in a 33 cm long, 7.94 cm inside diameter water-cooled Al_2O_3 tube through a matching network. The two plasmas were powered individually with slightly different frequency (table 1), each using a separate radio frequency (RF) power amplifier (ENI, model A500) driven by a function generator (Hewlett-Packard 3325A). Time averaged forward and reflected powers (defined as peak power \times duty cycle) were monitored by in-line power meters (Bird, model 43). Both sources were equipped with a copper Faraday shield to minimize capacitive coupling between the coil and the plasma. The voltage on the coil powering the plasma had measured $1/e$ rise and fall times of $\sim 3 \mu\text{s}$.

The plasma sources were separated by a 9.53 cm diameter grounded grid. Three different grids were used (see table 1): grid A was made of woven tungsten wire, and was 90% transparent with square holes 2.4 mm on a side. Grid B was also made of woven tungsten wire, and was 81% transparent with $230 \mu\text{m}$ square holes. Grid C, used for SF_6 , CF_4/O_2 and O_2 plasmas, was made of woven stainless steel wire (tungsten would be etched in F-atom containing plasmas) and was 68.9% transparent with 2.1 mm square holes. The grids were used to study the role of grid opening size on plasma ignition delay. A grid opening size larger than the sheath thickness would allow cross-talk between the two plasmas. For a grid opening size smaller than the sheath thickness, the two plasmas would be more isolated from one another. The grid also served as part of the grounded surface in contact with the plasma, to help minimize changes in the plasma potential during Langmuir probe measurements, when large electron currents were drawn.

Process gas was injected through a hole in the boundary electrode at the upper end of the auxiliary ICP and was pumped

Table 1. Base case parameters and range investigated.

Parameter	Base case	Range Investigated
RF frequency of main ICP	13.56 MHz	
RF frequency of auxiliary ICP	13.26 MHz	
Pulse frequency of main ICP	1 kHz	
Gas flow rate	25 sccm Cl ₂	25 sccm SF ₆ or 30 sccm O ₂ , or 30 sccm 80%CF ₄ /20%O ₂
Pressure	5 mTorr	2.5–20 mTorr
Duty cycle of pulsed main ICP	99%	20 %–99.9 %
Peak power of pulsed main ICP	500 W	100–500 W
CW power of auxiliary ICP	500 W	100–500 W
Metal grid	(A)	(A) 2.4 mm squares, 90% transparency (B) 230 μm squares, 81% transparency (C) 2.1 mm squares, 68.9% transparency

through the lower end of the main ICP by a 300 l s⁻¹ turbomolecular pump backed by a dry pump. Pressure (set by a throttle valve) was measured by a capacitance manometer (MKS 629, 100 mTorr full scale). Chlorine (25 sccm, Matheson 99.99% purity) was the main working gas, although other gases (25 sccm SF₆, 30 sccm O₂, or 30 sccm 80%CF₄-20%O₂) were used for some experiments. The pressure drop between the top of the upper source and the bottom of the lower source was estimated to be ~1 mTorr. The power supplied to the main ICP was pulsed at a frequency of 1 kHz (1000 μs pulse period), with variable duty cycle. The auxiliary ICP was powered continuously with a given power. Base case conditions (table 1) were: pressure = 5 mTorr, peak power to the main ICP = 500 W (13.56 MHz), and continuous wave (cw) power to the auxiliary ICP = 500 W (13.26 MHz).

Optical emission spectroscopy was used as a plasma diagnostic. A periscope consisting of two prisms was used to guide light from the plasma to the entrance slit of a monochromator with a 1200 grooves mm⁻¹ grating. The entrance slit opening was set to 1000 μm, which provided a resolution of about 2 nm. Light dispersed by the grating was detected by a GaAs photomultiplier tube (RCA C31034). The PMT current was measured by the voltage drop across a 3 kΩ load resistor, using an oscilloscope. The time constant of the circuit was ~0.3 μs, much smaller than the observed rise time of the plasma emission signal (10 μs). Atomic emission lines of Cl (837.5 nm; 4p ⁴D^o → 4s ⁴P), O (777.1 nm; 3p ⁵P → 3s ⁵S^o), and Ar (750.4 nm, 2p₁ Paschen series) were used to monitor the ignition and extinction of pulsed chlorine, oxygen, and argon plasmas. F emission at 685.6 nm (3p ⁴D^o → 3s ⁴P) was monitored in fluorine containing (SF₆ and 80% CF₄-20% O₂) plasmas.

A Langmuir probe (Scientific Systems Smartprobe, with modifications to reduce the probe size, as discussed in [24]) was used to measure electron and positive ion densities (n_e and n_+), electron temperature (T_e), and the electron energy probability function (EPPF). The cylindrical tungsten probe tip had a diameter of 0.18 mm and an exposed length of 6.5 mm. A reference electrode and RF chokes minimized distortion of the I - V characteristic due to any residual oscillations of the plasma potential. Fast data acquisition electronics enabled averaging of 100 s of I - V characteristics (at a given location and for given plasma conditions) to reduce noise. Plasma

parameters (n_e , n_+ , and T_e) were obtained by different procedures depending on the plasma electronegativity ($\alpha = n_-/n_e$), where n_- is the Cl⁻ number density. For a highly electronegative plasma ($\alpha \geq 1000$) that may form during the afterglow period, the plasma parameters were obtained by fitting the I - V curve and its second derivative using the procedure outlined by Bredin *et al* [25].

For lower plasma electronegativity, n_e and T_e were extracted from the EEPF. The EEPF is given by $f_p(\varepsilon) = \varepsilon^{-0.5} f(\varepsilon)$, where $f(\varepsilon)$ was obtained from the second derivative of the probe electron current I_e [1].

$$f(\varepsilon) = \frac{2m_e}{e^2 A} \sqrt{\frac{2\varepsilon}{m_e}} d^2 I_e / dV^2. \quad (1)$$

In equation (1), m_e is the electron mass, A is the probe exposed area, and e is the elementary charge. Voltage V is the applied probe voltage referenced to the plasma potential at the probe location. For a Maxwellian distribution of electron energies, a semi-log plot of $f_p(\varepsilon)$ versus ε yields a straight line. The electron density (n_e), and the average electron energy $\langle \varepsilon \rangle$ were calculated by integrating the electron energy distribution function $f(\varepsilon)$ as follows:

$$n_e = \int_0^\infty f(\varepsilon) d\varepsilon \quad (2)$$

$$\langle \varepsilon \rangle = \frac{1}{n_e} \int_0^\infty \varepsilon f(\varepsilon) d\varepsilon. \quad (3)$$

The effective electron temperature (T_e) was computed as $2/3\langle \varepsilon \rangle$. The ion density was obtained using Laframboise's orbital motion-limited (OML) theory for a collisionless sheath [26]:

$$n_i^+ = \xi \left(\frac{r_p}{\lambda_d}, \frac{V - V_p}{kT_e} \right) \frac{I_i^+}{eA} \sqrt{\frac{2\pi M_i}{kT_e}}, \quad (4)$$

where ξ is a correction factor that depends on a dimensionless potential and the ratio of cylindrical probe radius (r_p) to plasma Debye length (λ_d), I_i^+ is the ion saturation current, and M_i is the ion mass. To obtain time-resolved plasma properties, the probe was operated in 'boxcar' mode using an external trigger. Plasma parameters were collected on the discharge

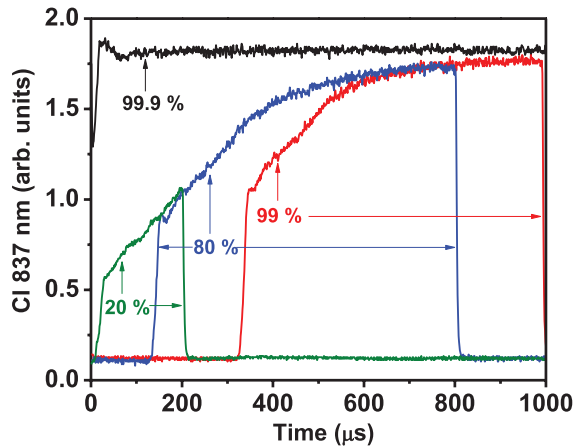


Figure 2. Optical emission intensity of the 837.5 nm line (Cl atoms) as a function of time during a pulse for different duty cycles. Other conditions were at their base case values (table 1).

axis ($r = 0$), in the main ICP, 110 mm below the grid separating the two sources (figure 1).

3. Results

3.1. Ignition delay versus duty cycle in chlorine plasmas

Plasma ignition and extinction as a function of time in chlorine plasmas were monitored using the Cl $\lambda = 837.5$ nm line emission intensity, as shown in figure 2. At the base case conditions (table 1), the auxiliary ICP was powered continuously with 500 W and the main ICP was pulsed at 1 kHz (period = 1000 μ s). The two plasmas were separated by a tungsten grid with either 2.4 mm or 230 μ m square holes (Grids A and B in table 1). RF power was delivered to the coil at $t \sim 0$ μ s, and remained on for a percent of the pulse period (duty cycle) that was varied from 20% to 99.9%. At 20% duty cycle, emission from Cl atoms appears within a few μ s after the plasma is turned on (i.e. no significant plasma ignition delay, beyond the 3 μ s rise time of the voltage on the coil). The emission intensity rises rather quickly at first, and continues to increase at a slower rate until the power is turned off at $t = 200$ μ s. At this time emission falls precipitously on the time scale of the decay of T_e (several μ s, see [9]). Similar behaviour was observed for duty cycles up to 60% (figure 3).

For duty cycles greater than 60%, however, a delay in plasma ignition was observed, i.e. the emission intensity was at the baseline level for significant amount of time after the power was switched on at $t = 0$. After this induction period, a rapid rise in emission signified plasma ignition (figure 2 for duty cycles of 80% and 99%). The ignition delay was found to increase almost linearly with duty cycle, for duty cycles larger than 70% (figure 3). A maximum ignition delay of ~ 320 μ s is observed for 99% duty cycle (plasma on/off time = 990/10 μ s). Further increase in duty cycle to 99.5% (plasma on/off time = 995/5 μ s) resulted in a nearly continuous plasma with no ignition delay. Generally, the ignition delay was found to be nearly independent of pressure in the 2.5–20 mTorr range investigated (figure 3).

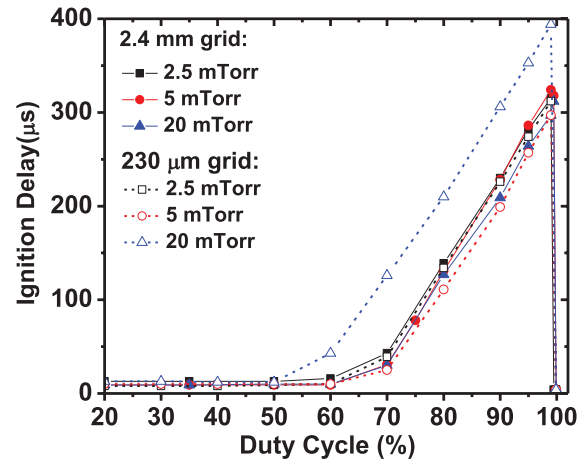


Figure 3. Plasma ignition delay versus duty cycle, for three different pressures and two different grids. Other conditions were at their base case values (table 1).

The increase in ignition delay with increasing duty cycle in chlorine ICPs is counter-intuitive. One would expect that, as the duty cycle increases, the shorter afterglow time (for constant pulse period) would cause the electron density at the end of the afterglow to be higher, making it easier to ignite the plasma, leading to a *shorter* delay time. For the same operating conditions, no ignition delays are observed in Ar plasmas, as shown by the time resolved optical emission measurements of the Ar $\lambda = 750.4$ nm line in figure 4.

Langmuir probe measurements were performed as a function of time for the same conditions and axial location used to collect optical emission. Figure 5 shows the electron density (n_e), positive ion density (n_+), and effective electron temperature (T_e) for a chlorine plasma, with peak main ICP power of 500 W, duty cycle of 20%, and auxiliary ICP cw power of 500 W. Under these conditions, little if any ignition delay is found. The dashed horizontal lines represent the electron density ($n_{e,aux}$), positive ion density ($n_{+,aux}$), and electron temperature ($T_{e,aux}$) in the main ICP, measured when *only* the auxiliary ICP is powered. For this low duty cycle, upon power turn-on of the main ICP at time $t = 0$ μ s, the electron density and electron temperature rise quickly (no ignition delay) and attain a quasi-steady value of $\sim 10^{11}$ cm^{-3} and ~ 4 eV, respectively. At $t = 200$ μ s, when the main ICP power is switched off, electrons are quickly lost due to dissociative attachment to Cl_2 molecules and diffusion to the walls, causing n_e to decrease rapidly, falling below $n_{e,aux}$ at $t \sim 230$ μ s. T_e initially decays rapidly from its quasi steady-state value of ~ 4 to ~ 2 eV in about 10 μ s after power is turned off, but while n_e keeps decreasing, T_e quickly turns around and reaches a relatively high value (~ 10 eV). The turnaround of T_e can be explained by the power injected into the main ICP from the auxiliary ICP. As n_e keeps decreasing, this power is distributed to a smaller number of electrons causing the temperature to heat up. This in turn causes ionization and the electron density starts increasing at $t \sim 250$ μ s. The power injected from the auxiliary ICP is now distributed to a larger number of electrons, causing a decrease in the electron temperature. On the other hand, n_+ decays smoothly from the start of the afterglow and, at $t \sim 400$

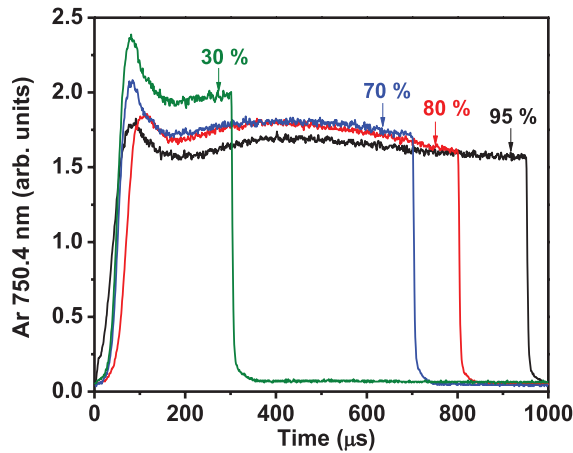


Figure 4. Optical emission intensity of the 750.4 nm line (Ar atoms) as a function of time during a pulse, for different duty cycles at otherwise base case conditions (table 1).

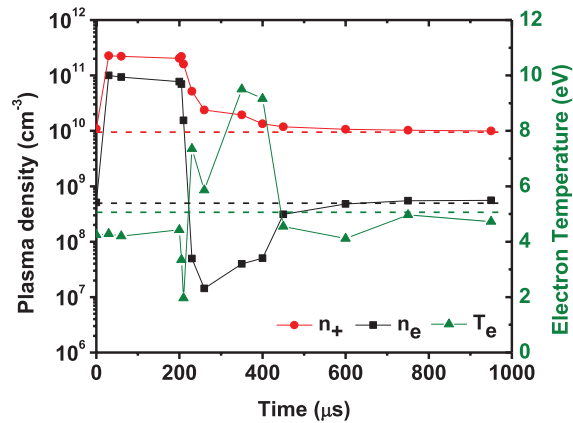


Figure 5. Positive ion density, electron density and electron temperature as a function of time during a pulse. Base case conditions (table 1), except duty cycle = 20%. Dashed lines correspond to the positive ion density ($n_{+,aux}$), electron density ($n_{e,aux}$) and electron temperature ($T_{e,aux}$) when only the auxiliary ICP is on (no power to the main ICP).

μs, n_+ reaches $n_{+,aux}$. When n_+ reaches $n_{+,aux}$, n_e increases to its quasi-steady value of $n_{e,aux}$, while T_e tends towards $T_{e,aux}$. It should be noted that late in a long afterglow of the main ICP, the plasma parameters are determined solely by the (cw powered) auxiliary ICP, injecting hot electrons into the main ICP.

Depending on conditions, an ion–ion plasma may form in the afterglow of the main plasma source. This ion–ion plasma is not ideal because of the presence of the auxiliary source. For example, the plasma potential of the ion–ion plasma formed in the afterglow was measured to be ~20V for $P_{aux} = 500$ W. Typically ion–ion plasmas have plasma potential close to zero because: (i) the electron density is extremely low, (ii) positive and negative ions have similar masses, thus similar diffusivities, yielding a near-zero space charge, and (iii) the plasma potential of an ion–ion plasma is determined by the ion temperature and not the electron temperature (as in conventional plasmas). In our case, the high plasma potential is due to the auxiliary plasma source operating continuously which may be thought of as a biased DC boundary electrode. It must be noted that relatively high ion temperatures (up to 2eV) were

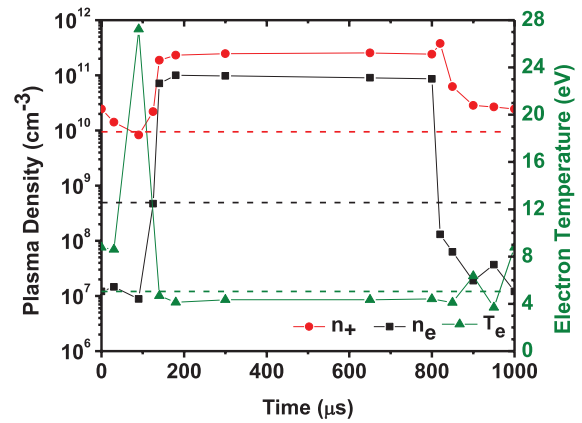


Figure 6. Positive ion density, electron density and electron temperature as a function of time during a pulse. Conditions were at base case (table 1), except that the duty cycle was 80%. Dashed lines correspond to the positive ion density ($n_{+,aux}$), electron density ($n_{e,aux}$) and electron temperature ($T_{e,aux}$) when only the auxiliary ICP is on (no power to the main ICP).

obtained by fitting the IV curves for highly electronegative afterglows. The Langmuir probe tip was about 2 cm away from a grounded stage (see figure 1). With the measured plasma potential ~20V, the electric field near the probe tip was ~10V cm⁻¹. Under such high electric fields it is reasonable to expect relatively high ion temperatures [27, 28].

Figure 6 shows n_e , n_+ and T_e for otherwise the same conditions as in figure 5, but with a duty cycle of 80%. n_e decays rapidly immediately after the main ICP power is turned-off at $t = 800$ μs. In contrast to figure 5 and consistent with Cl atomic emission intensity (figure 2), n_+ continues to decay, even after the power is turned back on at $t = 0$ μs, to start the next pulse cycle. Similar to the results in figure 5, as soon as n_e decreases below $n_{e,aux}$, the rate of further n_e decay slows down. At $t \sim 100$ μs, when n_+ reaches $n_{+,aux}$, n_e increases rapidly, and the main ICP ignites at $t = 140$ μs. An important difference between figure 5 (no plasma ignition delay) and figure 6 (plasma ignition delay), is that in figure 6 the afterglow is not long enough for the decaying ion density to reach $n_{+,aux}$. Similar behaviour was observed when the duty cycle was increased to 99% (figure 7). Extinguishing power at $t = 990$ μs causes n_e to decay rapidly. This decay continues (even after power is turned on at $t = 0$) until n_+ reaches $n_{+,aux}$ at $t \sim 250$ μs, whereupon n_e increases sharply, and the plasma ignites. For a duty cycle of 99.7% (not shown), when power to the main ICP was turned on, n_+ increased rapidly and reached a quasi-steady value of 2.5×10^{11} cm⁻³ while n_e reached a value of $\sim 6 \times 10^{10}$ cm⁻³. During the ~3 μs afterglow (here the afterglow is not clearly defined due to the ramp up and ramp down of voltage on the coil), n_+ decreased to 1.5×10^{11} cm⁻³, n_e decreased to 2×10^{10} cm⁻³, and the plasma ignited without delay when the power was turned on to start the next pulse cycle.

3.2. Ignition delay versus main and auxiliary ICP power

Figure 8 shows the plasma density and electron temperature obtained in the main ICP with an auxiliary source power of

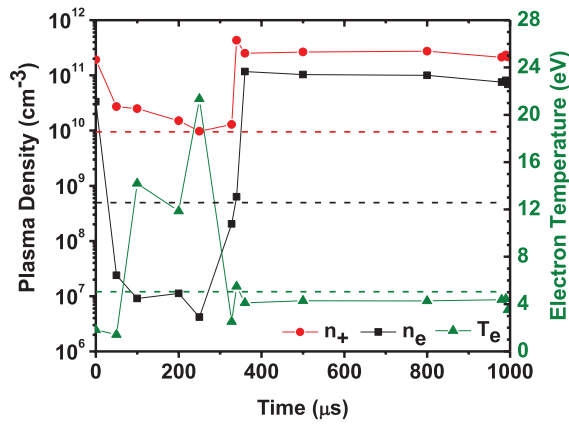


Figure 7. Positive ion density, electron density and electron temperature as a function of time during a pulse. Conditions were at base case (table 1). Dashed lines correspond to the positive ion density ($n_{+,aux}$), electron density ($n_{e,aux}$) and electron temperature ($T_{e,aux}$) when only the auxiliary ICP is on (no power to the main ICP).

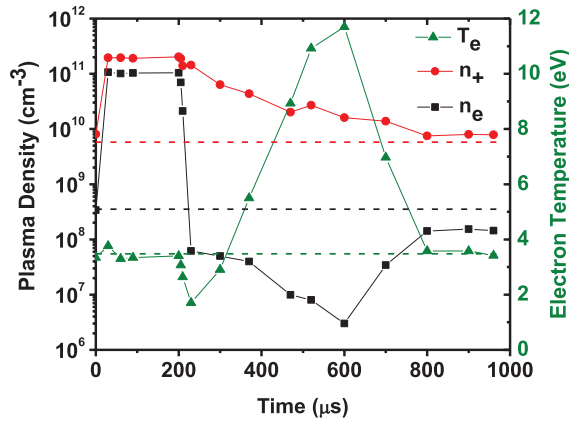


Figure 8. Positive ion density, electron density and electron temperature as a function of time during a pulse. Conditions were at base case (table 1), except that the duty cycle was 20% and the auxiliary cw power was 200W. Dashed lines correspond to the positive ion density ($n_{+,aux}$), electron density ($n_{e,aux}$) and electron temperature ($T_{e,aux}$) when only the auxiliary ICP is on (no power to the main ICP).

200W. Other conditions were as in figure 5. Immediately after the main ICP power is switched off at $t = 200 \mu s$, n_e decays by three orders of magnitude in about $30 \mu s$. Further decay of n_e is much slower compared to the case of 500W auxiliary ICP power (figure 5). At about $t = 600 \mu s$ ($400 \mu s$ into the afterglow), n_e starts increasing and eventually attains a value close to $n_{e,aux}$. The electron temperature reaches a maximum when n_e is at a minimum. Beyond that point T_e decreases until it is equal to $T_{e,aux}$. Meanwhile, n_+ decays until reaching $n_{+,aux}$. At this low duty cycle there is no plasma ignition delay. The plasma ignites promptly after power is turned on at $t = 0$.

The plasma ignition delay as a function of power to the auxiliary and main ICP is shown in figure 9. The duty cycle of the main ICP (with a 1 kHz pulse frequency) was kept constant at 99%, which gave the maximum ignition delay. For a peak power of 500W delivered to the main ICP, the time delay decreases from $600 \mu s$ to $330 \mu s$ (for the 2.4mm square grid), when the auxiliary ICP cw power is increased from 100 to

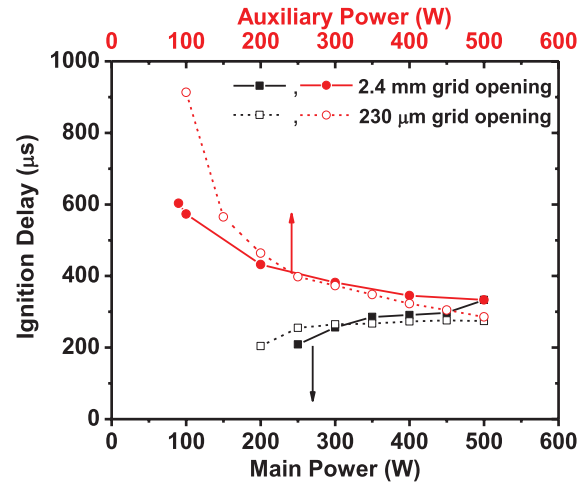


Figure 9. Black squares: ignition delay versus time-average power of main ICP. Red circles: ignition delay versus cw power of auxiliary ICP. Other conditions were at the base case values (table 1). Solid and open symbols correspond to grid A and grid B, respectively.

500W. With 500W cw power delivered to the auxiliary ICP, the time delay increases from $210 \mu s$ to $300 \mu s$ when the time-average power to the pulsed main ICP increases from 250W to 500W.

3.3. Effect of grid hole size

The size of the openings of the grid separating the two plasmas affects the degree of communication between the two plasmas. For a sheath thickness greater than the opening size, the two plasmas will be more isolated from one another, while for a sheath thickness less than the opening size, plasma will spill through the openings [29], and the two plasmas will be in ‘contact’ with each other. The Debye length of the main plasma ranges from $75\text{--}170 \mu m$ when only the auxiliary source is powered in the range 500–100W, at a pressure of 5 mTorr [30]. Early in the afterglow when the plasma electronegativity is high, the Debye length was estimated to be $50 \mu m$ for a 500W auxiliary ICP power. The sheath thickness is roughly $5 \times$ larger than the Debye length. To explore the effect of grid opening size on ignition delay, chlorine plasma experiments were conducted using tungsten grids A (2.4mm square openings) and B ($230 \mu m$ square openings). Figure 10 shows that the ignition delay as a function of duty cycle with 500W auxiliary power is about the same for both grids A and B. The ignition delay increases linearly with duty cycle beyond a threshold value, which depends on the power applied to the auxiliary ICP.

Figure 3 shows ignition delays as a function of duty cycle at three pressures, for grids A and B. At 2.5 mTorr, there is little, if any, dependence on grid opening size. At 5 mTorr, slightly shorter delays are found for grid B. At 20 mTorr, grid B produces substantially longer delays compared to grid A. The difference in the delay times produced by the two grids at 20 mTorr is nearly constant ($100 \mu s$), for duty cycles $\geq 70\%$. Ignition delays as a function of power to the auxiliary and main ICP for grids A and B are compared in figure 9. Relatively

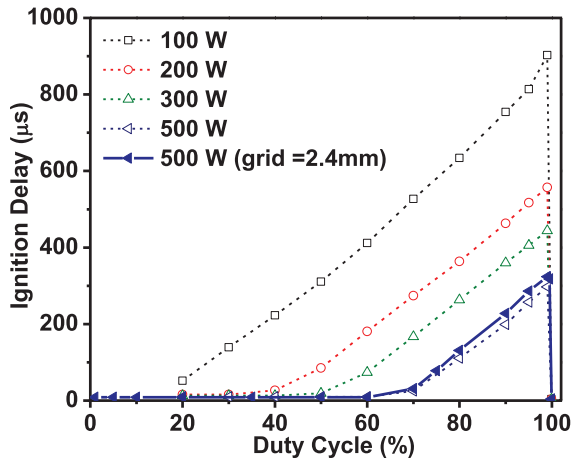


Figure 10. Plasma ignition delay versus duty cycle, with different auxiliary ICP cw powers. Open symbols: grid B. Solid symbol: grid A. Pressure, flow rates, and main ICP peak power were at base case values (table 1).

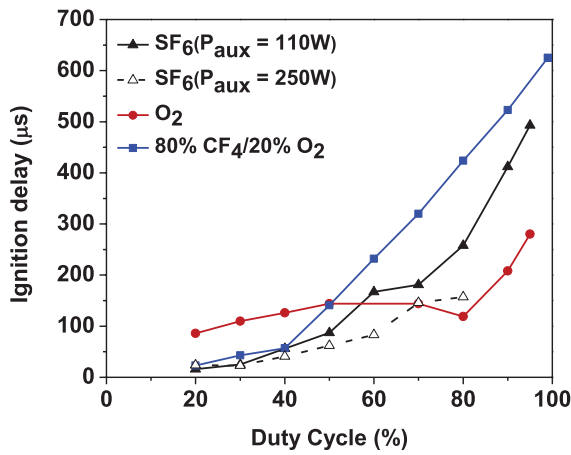


Figure 11. Plasma ignition delay versus duty cycle in different electronegative gases. The main ICP was pulsed with a pulse repetition frequency of 1 kHz. Grid C was used and the pressure was 5 mTorr. The main ICP peak power/auxiliary ICP cw power was: SF₆ (400 W/110 W or 400 W/250 W), O₂ (300 W/100 W), and 80%CF₄-20%O₂ (450 W/110 W).

subtle differences are found with the exception of the lowest auxiliary power (100 W) for which grid B produces ~300 μs longer delays in plasma ignition. This may be a result of a thicker sheath (~850 μm) at low power, increasing the isolation between the two plasmas.

3.4. Ignition delays in other electronegative gas plasmas

Plasma ignition delays, measured by optical emission, were also observed in other electronegative gases (SF₆, O₂, or 80%CF₄-20%O₂). Figure 11 shows the ignition delay as a function of duty cycle, for pulsed plasmas (1 kHz pulse frequency) in different electronegative gases. Similar to Cl₂ plasmas, ignition delays increase as a function of duty cycle above a threshold (with O₂ being a possible exception between 50% and 80% duty cycle).

The ignition delay as a function of power to the auxiliary and main ICP in SF₆ is shown in figure 12. Unfortunately, due

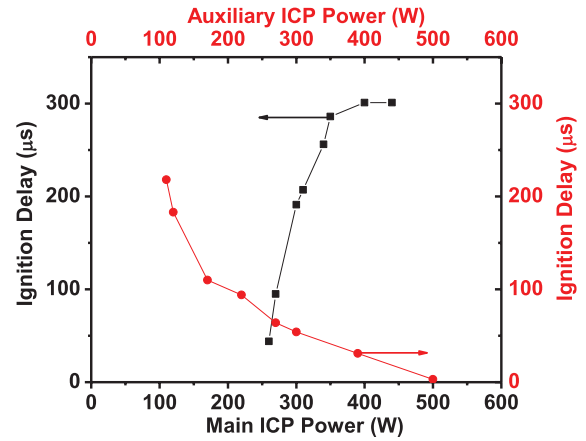


Figure 12. Black symbols, left axis: ignition delay versus time-average power of main ICP in SF₆ plasmas. The main ICP power was pulsed with at 1 kHz and 80% duty cycle. The auxiliary ICP was supplied with 110 W cw power. Red symbols, right axis: ignition delay versus cw power of auxiliary ICP. The main ICP was pulsed with at 1 kHz, 80% duty cycle, and 320 W time-average power. For all data points, grid C was used, and the pressure was 5 mTorr.

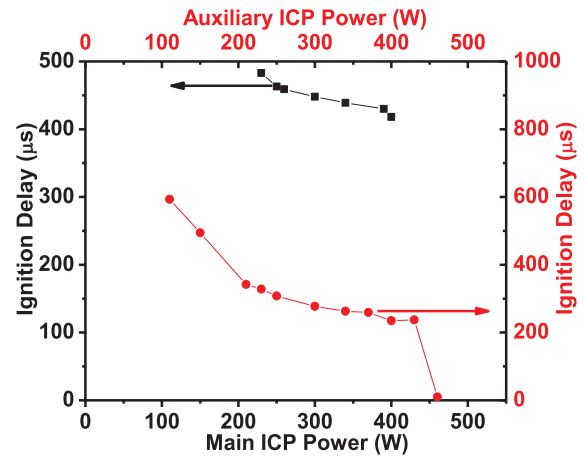


Figure 13. Black symbols, left axis: ignition delay versus time-average power of main ICP in 80%CF₄-20%O₂ plasmas. The main ICP was pulsed with at 1 kHz and 80% duty cycle. The auxiliary ICP was supplied with 110 W cw power. Red symbols, right axis: Ignition delay versus cw power of auxiliary ICP. The main ICP was pulsed with a frequency of 1 kHz, 99% duty cycle, and 450 W time-average power. For all data points, grid C was used, and the pressure was 5 mTorr.

to experimental constraints, it was not possible to operate at the duty cycle and power levels used for Cl₂ in figure 9, so a direct comparison cannot be made. Nonetheless the trends are similar, in that at constant average power to the main ICP, the ignition delay decreases with increasing auxiliary ICP power, while the delay increases with increasing main ICP power. Note that the increase in delay with main ICP power in SF₆ is much stronger than that in Cl₂.

The ignition delay was also found to decrease with increasing auxiliary ICP power in CF₄/O₂ plasmas (figure 13) and O₂ plasmas (figure 14). Contrary to Cl₂ and SF₆, however, the ignition delay *decreases* (slightly for CF₄/O₂ and drastically for O₂) with increasing average power delivered to the

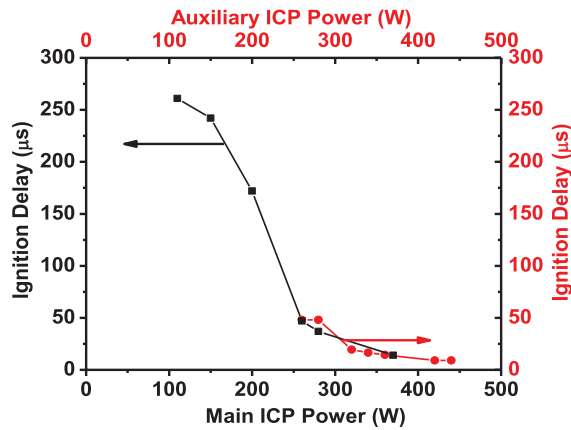


Figure 14. Black symbols, left axis: ignition delay versus time-average power of main ICP in O_2 plasmas. The main ICP was pulsed with at 1 kHz and 90% duty cycle. The auxiliary ICP was supplied with 110W cw power. Red symbols, right axis: Ignition delay versus cw power of auxiliary ICP. The main ICP was pulsed with a frequency of 1kHz, 90% duty cycle, and 250W time-average power. For all data points, grid C was used, and the pressure was 5 mTorr.

main ICP. If the plasma becomes less electronegative with increasing power, then the delay will be shortened (note again that Ar plasmas exhibit no ignition delay). On the other hand, if the electronegativity increases with power because a more attaching product is formed, then the ignition delay would be lengthened (see below).

4. Discussion

With the main pulsed ICP operating in tandem with a continuously powered auxiliary ICP, it is possible to ignite a 1 kHz pulsed plasma at the end of an 800 μs afterglow period (20% duty cycle), with little or no ignition delay. This is due to a background electron density, $n_{e,aux}$, in the main ICP, established by a plasma flux injected from the auxiliary ICP, balancing plasma loss during the afterglow (power = 0) in the main chamber. In this case, a sudden jump in n_e is observed at $t = 400 \mu s$ (figure 5) before the plasma density and electron temperature settle at their values ($n_{e,aux}$ and $T_{e,aux}$) measured with *only* the auxiliary power on. This situation is reminiscent of the findings of Malyshev and Donnelly (M&D) [31]. They studied the dynamics of a 10 mTorr chlorine pulsed ICP (300W average power, pulse frequency of 333.33 Hz to 10kHz, 50% duty cycle, no Faraday shield), with and without RF bias power applied on a substrate stage. Without bias power on the stage, plasma ignition always occurred without delay and T_e exhibited the expected overshoot when power was turned on, before reaching a (quasi)steady-value of 2.5 eV for the remainder of the active glow. Since there was no Faraday shield in the M&D experiment, plasma ignition was facilitated by capacitive coupling from the RF coil. When the afterglow was made sufficiently long (i.e. 500 to 3000 μs), however, and RF bias was applied *continuously* to the stage, n_+ decayed until reaching the constant value sustained by bias power alone (referred to as the ion density in the ‘reactive ion etching (RIE) mode’, analogous to $n_{+,aux}$ of the present work).

Meanwhile n_e decayed to well below the electron density produced in the RIE mode (analogous to $n_{e,aux}$ here).

In the present work, the auxiliary ICP source plays the role of the RF biased stage, in the sense that plasma injection from the auxiliary to the main ICP can maintain a low density plasma in the main ICP, when *only* the auxiliary ICP is powered. It is also seen that lowering the power of the auxiliary source increases the time for electron density to build up later in the afterglow (200 μs for 500W auxiliary power compared to 500 μs for 200W auxiliary power), which is similar to what M&D observed by varying the ICP source and stage RF bias power.

The time-dependent behaviour of n_+ , n_e and T_e in the main ICP, during the transition from the pulsed-power-sustained mode to the auxiliary-plasma-sustained mode (APS-mode) in the present work (as well as the transition to the RIE-mode in the work of M&D), can be understood by considering the behaviour of positive ions, combined with the partitioning of a constant electron energy density flux (from the auxiliary source) to a decaying electron density (in the main source). After the power of the main ICP is switched off (in the afterglow), n_e drops rapidly, due to loss of electrons by dissociative attachment and diffusion to the walls. On the other hand, the influx of hot electrons from the auxiliary plasma to the main ICP increases the temperature of the residual electrons in the main ICP, since the electron energy is distributed among a small number of electrons. The high T_e promotes gas ionization and the electron density decay rate decreases, but n_+ is still large enough that the ion and electron losses to the walls by diffusion are larger than the rate of electron-ion pair production. Thus, n_e remains below $n_{e,aux}$. When n_+ reaches $n_{+,aux}$, the ionization rate exceeds the loss rate, and n_e increases rapidly as the plasma switches to the APS mode. If the afterglow is long enough for the decaying n_+ to reach $n_{+,aux}$ during the afterglow, then there is no plasma ignition delay (figure 5). If the afterglow is too short for n_+ to reach $n_{+,aux}$ then there is plasma ignition delay (figures 6 and 7).

Under conditions for which a long delay time is observed before plasma ignition, a similar effect appears to be occurring. The plasma cannot ignite until n_+ reaches $n_{+,aux}$, while n_e is free to decrease below $n_{e,aux}$. Once the power is off for more than a few μs , the drop in T_e causes a rapid increase in the electron attachment rate by Cl_2 causing a swift drop in n_e . This leads to a reduced efficiency in inductive coupling when the power is turned back on. In addition, the matching network is tuned to deliver maximum net power at or near the (quasi) steady maximum electron density reached close to the end of the power-on (active glow) period. Hence, the power transfer efficiency is further reduced due to poor impedance-matching conditions. As a result, the plasma continues to decay. When n_+ reaches $n_{+,aux}$, n_e jumps to $n_{e,aux}$. At this point, the inductive power coupling, though still inefficient, produces ionization that then improves the inductive power coupling efficiency, quickly leading to increasing plasma density, as the ICP ignites.

The higher the duty cycle, the higher the positive ion density at the end of the afterglow, the longer it takes for n_+ to reach $n_{+,aux}$, and the longer it takes for ignition to occur

(figure 3). Also, the higher the power to the auxiliary ICP, the larger the value of $n_{+,aux}$, and the shorter the time for n_+ to decay to $n_{+,aux}$ (figure 9). Raising the power to the main ICP results in higher plasma density at the end of the active glow, resulting in longer delays before n_+ decays to the value of $n_{+,aux}$ (figure 9).

The flux of electrons from the auxiliary ICP to the main ICP may be altered by using different grid openings as discussed earlier (section 3.3). At a pressure of 5 mTorr and for the grid with small openings (grid B, table 1) longer ignition delays are observed especially at lower auxiliary ICP powers (100–200 W) (figure 10). This may be due to the larger sheath thickness at lower auxiliary powers, increasing the isolation between the two plasmas (by preventing plasma leakage through the grid holes) and reducing the flux of electrons from the auxiliary ICP into the main ICP.

The delay times measured as a function of main ICP and auxiliary ICP power in SF₆ plasmas follow a similar trend as in Cl₂ plasmas. However, the effect of lowering the main ICP power or increasing the auxiliary power is more dramatic in the SF₆ plasmas. In the case of O₂ plasmas it was noted that delay times decreased with increasing main ICP power. This may be attributed to decreased plasma electronegativity of the oxygen discharge with increasing power. Increasing power results in higher densities of O₂ (¹Δ_g) which reacts with O⁻ to form ozone, and also detaches O₂⁻ [32]. Destruction of negative ions reduces the plasma electronegativity and, therefore, the delay time decreases with increasing main ICP power.

5. Summary

Faraday shielded pulsed electronegative plasmas are often difficult to ignite because electrons can be rapidly lost in the afterglow by attachment to gas molecules and diffusion to the plasma containing walls, requiring large capacitive fields to ignite the plasma, which the Faraday shield prevents. A dual plasma source, consisting of a main inductively coupled plasma (ICP), in tandem with an auxiliary ICP, was developed to overcome this difficulty. The Faraday shielded sources were separated by a grounded metal grid. The main ICP power was pulsed with a frequency of 1 kHz, while the auxiliary ICP operated in continuous wave (cw) mode, injecting hot electrons through the grid to ignite the main ICP. Interestingly, for a certain set of conditions, the plasma ignited with a time delay after the RF power to the main ICP was turned on to start the next cycle. In pulsed chlorine plasmas, ignition delay appeared after a threshold value of the duty cycle (60% for the base case experimental conditions used) and, contrary to expectation, the ignition delay was longer with increasing duty cycle up to ~99.5% with no delay at a duty cycle of ~99.7%.

Langmuir probe diagnostics were employed to measure the time evolution of electron and positive ion densities as well as electron temperature. During the afterglow (main power off) of a pulsed chlorine plasma, it was observed that the electron density decayed rapidly. At the same time, the positive ion density decayed at a substantially slower rate. The time during the afterglow when the positive ion density (n_+) in the main

ICP decayed to the value $n_{+,aux}$, obtained when *only* the auxiliary ICP was powered, was of critical importance. When n_+ reached $n_{+,aux}$, the electron production rate exceeded the electron loss rate due predominantly to gas ionization promoted by hot electron injection from the auxiliary plasma to the main ICP, and to a much smaller extent by very inefficient inductive coupling. At this point, n_e increased, which improved the inductive power coupling efficiency, further increasing the rate of production of electron–ion pairs, igniting the plasma. If the afterglow was long enough for the decaying n_+ to reach $n_{+,aux}$ during the afterglow, then there was no plasma ignition delay. If the afterglow was too short for this to occur, then plasma ignition was delayed. These findings parallel the observations of Malyshev and Donnelly ([31]). The auxiliary ICP in the present experiment plays the role of an RF biased stage in M&D's separately powered ICP.

The plasma ignition delay could be varied by changing the power of the auxiliary source and the main source. At higher auxiliary powers (i.e. higher $n_{+,aux}$), the ignition delay was found to be smaller due to the shorter time required for n_+ to decay to $n_{+,aux}$. At higher main ICP powers (i.e. higher n_+), the ignition delay was found to increase due to the longer time required for n_+ to decay to $n_{+,aux}$.

Besides chlorine, ignition delays were also observed in other electronegative gases such as SF₆, 80% CF₄–20% O₂, and O₂. The ignition delay trends as a function of duty cycle, auxiliary and main power, were similar to those in chlorine. In 80% CF₄–20% O₂ and O₂ plasmas, however, the ignition delay was found to decrease with increasing main ICP power. This may be due to the role of O₂ (¹Δ_g) in making the plasma less electronegative, by providing additional pathways (associative detachment of O⁻ and electron detachment from O₂) for negative ion loss which cause the ignition delay to decrease with increasing main ICP power. No ignition delays were observed in electropositive (e.g. Ar) plasmas.

Acknowledgments

This work was supported by the Department of Energy, Office of Fusion Energy Science, contract DE-SC0001939, and the National Science Foundation grant 150518.

References

- [1] Lieberman M A and Lichtenberg A J 2005 *Principles of Plasma Discharges and Materials Processing* (Hoboken, NJ: Wiley)
- [2] Banna S, Agarwal A, Cunge G, Darnon M, Pargon E and Joubert O 2012 Pulsed high-density plasmas for advanced dry etching processes *J. Vac. Sci. Technol. A* **30** 040801
- [3] Donnelly V M and Kornblit A 2013 Plasma etching: yesterday, today, and tomorrow *J. Vac. Sci. Technol. A* **31** 050825
- [4] Economou D J 2014 Pulsed plasma etching for semiconductor manufacturing *J. Phys. D: Appl. Phys.* **47** 303001
- [5] Verdeyen J T, Beberman J, and Overzet L 1990 Modulated discharges—effect on plasma parameters and deposition *J. Vac. Sci. Technol. A* **8** 1851–6
- [6] Ramamurthi B and Economou D J 2002 2D pulsed-plasma simulation of a chlorine discharge *J. Vac. Sci. Technol. A* **20** 467–78

- [7] Overzet L J, Lin Y and Luo L Z 1992 Modeling and measurements of the negative-ion flux from amplitude modulated rf discharges *J. Appl. Phys.* **72** 5579–92
- [8] Midha V and Economou D J 2000 Spatio-temporal evolution of a pulsed chlorine discharge *Plasma Sources Sci. Technol.* **9** 256–69
- [9] Malyshev M V, Donnelly V M, Colonell J I and Samukawa S 1999 Dynamics of pulsed-power chlorine plasmas *J. Appl. Phys.* **86** 4813–20
- [10] Kanakasabapathy S K, Overzet L J, Midha V and Economou D 2001 Alternating fluxes of positive and negative ions from an ion–ion plasma *Appl. Phys. Lett.* **78** 22–4
- [11] Kaganovich I D, Ramamurthi B N and Economou D J 2001 Spatiotemporal dynamics of charged species in the afterglow of plasmas containing negative ions *Phys. Rev. E* **64** 036402
- [12] Subramonium P and Kushner M J 2001 Pulsed inductively coupled chlorine plasmas in the presence of a substrate bias *Appl. Phys. Lett.* **79** 2145–47
- [13] Sugai H, Nakamura K, Hikosaka Y and Nakamura M 1995 Diagnostics and control of radicals in an inductively-coupled etching reactor *J. Vac. Sci. Technol. A* **13** 887–93
- [14] Malyshev M V, Donnelly V M, Downey S W, Colonell J I and Layadi N 2000 Diagnostic studies of aluminum etching in an inductively coupled plasma system: determination of electron temperatures and connections to plasma-induced damage *J. Vac. Sci. Technol. A* **18** 849–59
- [15] Samukawa S and Terada K 1994 Pulse-time modulated electron-cyclotron-resonance plasma-etching for highly selective, highly anisotropic, and less-charging polycrystalline silicon patterning, *J. Vac. Sci. Technol. B* **12** 3300–305
- [16] Samukawa S, Ohtake H and Mieno T 1996 Pulse-time-modulated electron cyclotron resonance plasma discharge for highly selective, highly anisotropic, and charge-free etching *J. Vac. Sci. Technol. A* **14** 3049–58
- [17] Ahn T H, Nakamura K and Sugai H 1996 Negative ion measurements and etching in a pulsed-power inductively coupled plasma in chlorine *Plasma Sources Sci. Technol.* **5** 139–44
- [18] Shin H, Zhu W, Xu L, Donnelly V M and Economou D J 2011 Control of ion energy distributions using a pulsed plasma with synchronous bias on a boundary electrode *Plasma Sources Sci. Technol.* **20** 055001
- [19] Wang Y, Benck E C, Misakian M, Edamura M and Olthoff J K 2000 Time-resolved measurements of ion energy distributions and optical emissions in pulsed radio-frequency discharges *J. Appl. Phys.* **87** 2114–121
- [20] Tuszewski M 1996 An electronegative inductive discharge instability *J. Appl. Phys.* **79** 8967–75
- [21] Lieberman M A, Lichtenberg A J and Marakhtanov A M 1999 Instabilities in low-pressure inductive discharges with attaching gases *Appl. Phys. Lett.* **75** 3617–19
- [22] Despiau-Pujo E and Chabert P 2009 Global model of instabilities in low-pressure inductive chlorine discharges *Plasma Sources Sci. Technol.* **18** 045028
- [23] Chabert P, Lichtenberg A J, Lieberman M A and Marakhtanov A M 2001 Instabilities in low-pressure electronegative inductive discharges *Plasma Sources Sci. Technol.* **10** 478
- [24] Liu L, Sridhar S, Zhu W, Donnelly V M, Economou D J, Logue M D and Kushner M J 2015 External control of electron energy distributions in a dual tandem inductively coupled plasma *J. Appl. Phys.* **118** 083303
- [25] Bredin J, Chabert P and Aanesland A 2013 Langmuir probe analysis of highly electronegative plasmas *Appl. Phys. Lett.* **102** 154107
- [26] Steinbrüchel C 1990 A new method for analyzing Langmuir probe data and the determination of ion densities and etch yields in an etching plasma *J. Vac. Sci. Technol. A* **8** 1663–67
- [27] Ellis H W, Pai R Y, McDaniel E W, Mason E A and Viehland L A 1976 Transport properties of gaseous ions over a wide energy range *At. Data Nucl. Data Tables* **17** 177–210
- [28] Phelps A V 1991 Cross sections and swarm coefficients for nitrogen ions and neutrals in N₂ and argon ions and neutrals in Ar for energies from 0.1 eV to 10 keV *J. Phys. Chem. Ref. Data* **20** 557–73
- [29] Kim C-K and Economou D J 2002 Plasma molding over surface topography: Energy and angular distribution of ions extracted out of large holes *J. Appl. Phys.* **91** 2594–603
- [30] Economou D J 2007 Fundamentals and applications of ion–ion plasmas *Appl. Surf. Sci.* **253** 6672–80
- [31] Malyshev M V and Donnelly V M 2000 Dynamics of inductively-coupled pulsed chlorine plasmas in the presence of continuous substrate bias *Plasma Sources Sci. Technol.* **9** 353
- [32] Belostotsky S G, Economou D J, Lopaev D V and Rakhimova T V 2005 Negative ion destruction by O(³P) atoms and O₂ (*a* ¹Δ_g) molecules in an oxygen plasma *Plasma Sources Sci. Technol.* **14** 532